Modelling the impact of soot fractal aggregate structures on the aerodynamic and mobility diameters of particles in the transition regime

C. Jourdain, Prof. A. M. Boies (University of Cambridge) – Dr. J. P. Symonds (Cambustion Ltd)

UNIVERSITY OF CAMBRIDGE

Aerosol CDT Annual Conference – 06/07/22

CAMBUSTION

Background and motivation

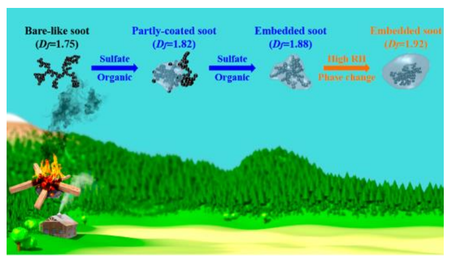

Figure 1: Soot aging in the atmosphere [1]

- The ageing process, i.e. soot maturing in the atmosphere, usually involves partial or total coating by water or organic compounds (Fig. 1). This added material drastically changes the radiative transfer to/from the in-flight particles and their overall morphology and dynamics [1]

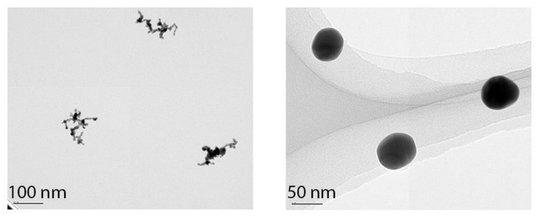

Figure 2: TEM image of Au nanoparticles: original (left), sintered (right) [2]

- Fractal nanoparticles are often formed within high-temperature chambers where, after inception, larger particles and clusters aggregate and commonly overlap (Fig. 2) [2]

True properties of fractal nanoaggregates can be recovered experimentally using a combination of:

- Particle generation (miniCAST, powder…)
- Particle processing, e.g. collisional/condensational growth, charging, heating, sintering
- Particle measurement: mass (CPMA), aerodynamic diameter (AAC), mobility diameter (DMA)

At the same time, there is a need for a fully embedded numerical tool to estimate aerosol properties of fractal aggregates in real scenarios – which unlocks common assumptions such as spherical particle shape, non-continuum effects, charging uniformity… – to allow comparisons with aerosol instrumentation data

Model description

This three-dimensional semi-stochastic model is composed of four modules:

- Generation
- Processing
- Visualisation
- Computation of properties

Generation

A tuning sequential aggregation approach is chosen [3] to produce quasi-fractal aggregates in agreement with the equation: $N = k_f \left(2R_g/d_{pp}\right)^{D_f}$

The two-step model proceeds as follows:

- **Step 1** – Particle-Cluster aggregation: two particles form a dimer and subsequent single particles collide and stick to the original cluster; a constant sub-cluster size N_{sub} = 8 is chosen.
- **Step 2** – Cluster-Cluster aggregation: candidate sub-clusters generated as above are selected and matched (see Fig. 3) such that the correct fractal parameters are satisfied according to:

$$D_{cm} = \sqrt{\left(m^2 R_g^2 - m\left(m_1 R_{g1}^2 + m_2 R_{g2}^2\right)\right)/(m_1 m_2)}$$

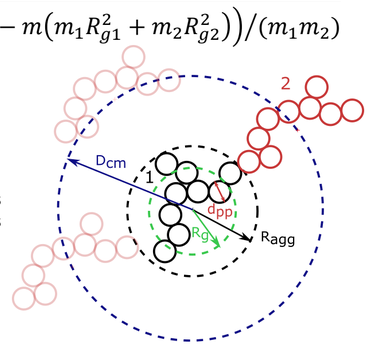

Figure 3: Sub-clusters aggregation trials

Processing

Processing phenomena of interest include particle overlapping and coating:

- The overlap is achieved with a shift in particle positions with $0 < c_{ov} < 1$
- Nanoparticle coating is restricted to the formation of pendular rings between monomers, mimicking the mass transfer from vapour to liquid condensate in a subsaturated environment. The surfaces of constant mean curvature (H) are described here using the 2-D axisymmetric Young-Laplace theory, satisfying:
  - A negative nodoidal surface for S < 1 (H < 0)
  - A catenoidal surface for S = 1 (H = 0)
- The wetting behaviour is affected by the contact angle (theta) formed between the liquid/gas and liquid/solid interfaces in the system, a small theta value indicating favourable wetting

Visualisation

The final aggregate can be visualised via:

- 3-D manipulation embedded in the software
- Black and white micrograph, enabling further comparison with microscopy data (Fig. 4)

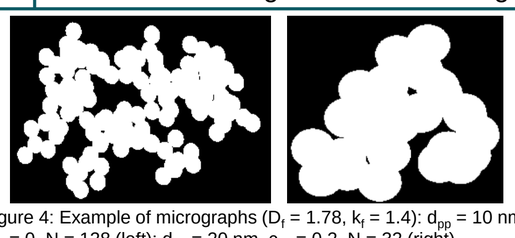

Figure 4: Example of micrographs (D_f = 1.78, k_f = 1.4): d_{pp} = 10 nm, c_{ov} = 0, N = 128 (left); d_{pp} = 20 nm, c_{ov} = 0.2, N = 32 (right)

Computation of properties

- The Knudsen number is calculated as $Kn = \pi R_s/PA$, where PA is the orientationally-averaged projected area (N_{orient} = 500) and R_s the Smoluchowski radius
- R_s is calculated via the Brownian walker method [4]
- The charging state in assumed to be +1, the mobility is then $Z = eB$, B being the mechanical mobility
- The mobility diameter (d_m) is calculated by solving

$$Z - \left(\frac{e}{3\pi\mu d_m}\right)\left(1 + \frac{2\lambda}{d_m}\left(1.257 + 0.4\exp\left(\frac{-0.55 d_m}{\lambda}\right)\right)\right) = 0$$

and the aerodynamic diameter is inferred following [5]

$$\tau - \left(\frac{\rho_0 {d_{ae}}^2}{18\mu}\right)\left(1 + \frac{2\lambda}{d_{ae}}\left(1.257 + 0.4\exp\left(\frac{-0.55 d_{ae}}{\lambda}\right)\right)\right) = 0$$

where τ is the relaxation time $\tau = mB$, m being the total mass

- The effective density is defined as $\rho_{eff} = \frac{6m}{\pi d_m^3}$

Aggregate generation

Fractal dimension (D_f, k_f)

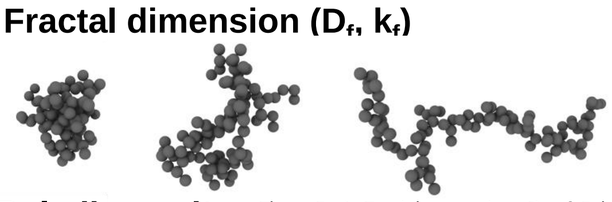

The fractal parameters represent the compactness of the structure and range from 1 (lacy) to 3 (compact)

Figure 5 - A: Fractal parameters: D_f = 2.5, k_f = 0.7 (left), D_f = 1.78, k_f = 1.4 (middle), D_f = 1.3, k_f = 2.0 (right)

Polydispersity

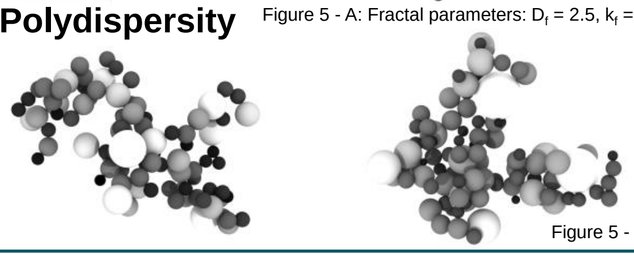

The polydispersity is introduced by sampling the primary particle diameters from a log normal distribution

Figure 5 - B: Polydispersity: σ = 1.3 (left), σ = 1.8 (right)

Theoretical framework

The dynamics of in-flight nanoparticles is significantly dependent on the flow regime established with regards to the surrounding gas molecules. This is represented by the non-dimensional Knudsen number (Kn)

- Kinetic and diffusion mechanisms agree reasonably well with experiments in the free molecular and continuum regimes, respectively
- A large proportion of fine and ultrafine particles, however, falls in the transition regime, where finding a characteristic length is not straightforward and simplified theories give rise to strong discrepancies

Results

Polydispersity

- Fractal aggregates with D_f = 1.78 , k_f = 1.4, d_{gm} = 10 nm
- Each data point represents between 50 to 100 simulations
- Kn = 0.6 – 3.5

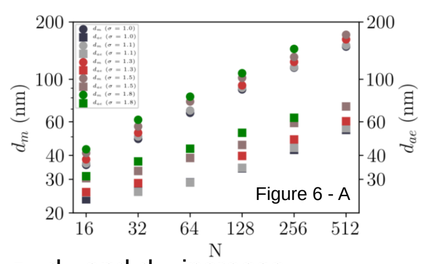

- d_m and d_{ae} increase monotonically (linearly in semi-log space) (Fig. 6-A)
- Higher polydispersity leads to larger d_m and d_{ae}

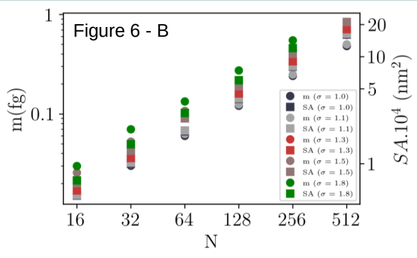

- Polydisperse aggregates have more mass and surface than their monodisperse counterparts (Fig. 6-B)

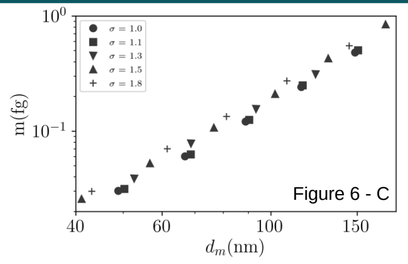

- The mass-mobility relation is shifted toward higher masses for polydisperse aggregates in the entire mobility range (Fig. 6-C)

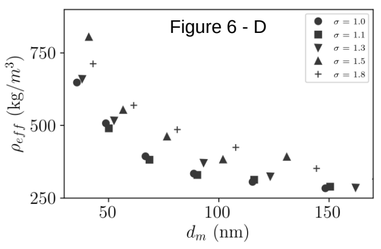

- The effective density converges towards a lower limit $\rho_{eff,final}$ = 24-49% $\rho_{eff,init}$ (Fig. 6-D)
- Observations agree with litterature [6]
- Denser structures arise from an increase in polydispersity

Near power laws: $d_{ae} = 11.343N^{0.2404}$ (σ = 1.0) and $d_{ae} = 15.347N^{0.2538}$ (σ = 1.8)
$d_m = 11.737N^{0.4114}$ (σ = 1.0) and $d_m = 13.457N^{0.4297}$ (σ = 1.8)

Overlap

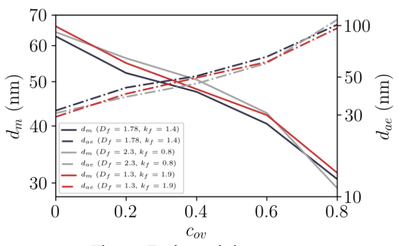

Figure 7: d_m and d_{ae} v. c_{ov} for different fractal parameters

- A simplified overlap implementation is used here, i.e. without mass redistribution<
- The value c_{ov} = 0 represents the point contact configuration while for c_{ov} = 1, the aggregate is completely spherical
- A critical overlap coefficient exists for which the aerodynamic and mobility diameters are equal
- This event is delayed for more compact aggregates

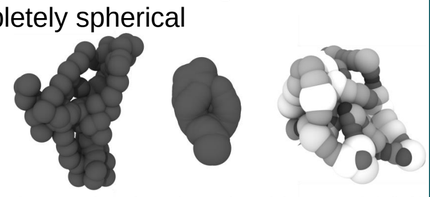

Figure 8: Examples of overlapped particles: c_{ov} = 0.2 (left), c_{ov} = 0.9 (middle), c_{ov} = 0.5 with σ = 1.3 (right)

Sub-saturated environment: capillary condensation

- At low saturation, MD simulations on Cu dimers show that water molecules condense on solid surfaces via two mechanisms: adsorption in the gap, forming a bridge, and adsorption + surface diffusion towards the bridge on convex surfaces (Fig. 9)

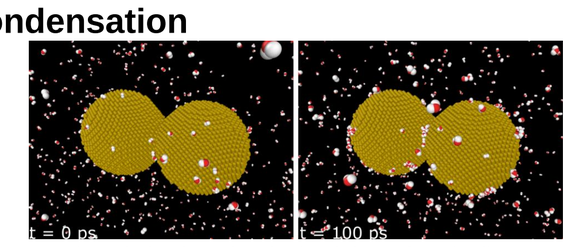

Figure 9: Condensation simulated via MD for a Cu dimer with $T_{vap} \simeq$ 500 K and T_{solid} = 300 K

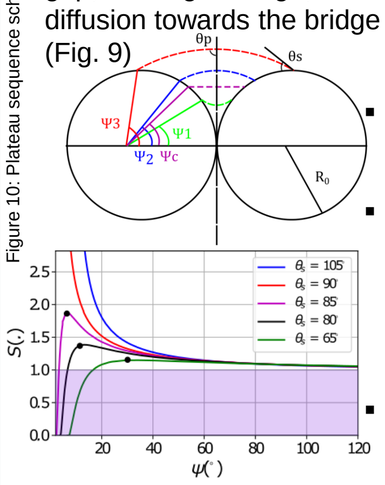

Figure 10: Plateau sequence schematic

Figure 11: Saturation v. filling angle for different θ_s

- Pendular rings are formed between monomers and evolve following the Plateau sequence as the filling angle (ψ) is increased (Fig. 10)
- Figure 11 shows that a critical value of the contact angle ($\theta_{s,crit}$) exists below which capillary condensation may exist ($\theta_s \leq 85°$ in this study using water, see purple region). For highly hydrophobic systems with $\theta_s > \theta_{s,crit}$ there may activation by droplet nucleation on solid surfaces instead of activation via pendular rings
- This simplified theory is useful in the capillary condensation regime but fails once the critical saturation (black dots) is reached, triggering uncontrollable growth and further coating surface interaction

Application of the model using different coating materials on an aggregate with properties D_f = 1.78, k_f = 1.4, N = 64, d_{pp} = 10 nm

- For S < 1, the d_m of coated particles remains quasi-unchanged and its average value d_{mav} can be taken constant. Instead, d_{ae} increases drastically as the total mass of the coated aggregate increases (Fig. 12)

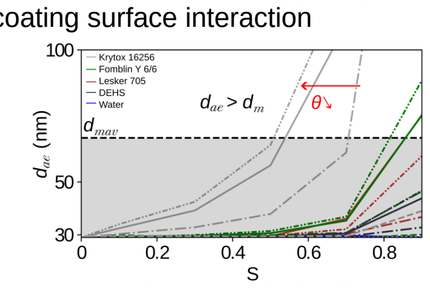

Figure 12: d_{ae} v. saturation for different θ_s

- In this application case, d_m always remains higher than d_{ae} in the subsaturated range for water, DEHS, and Lesker 705
- For systems with θ ≤ 40° and using heavy oils (Krytox 16256, Fomblin Y6/6) as coating materials, there is a critical saturation point (S_{crit}) where $d_m = d_{ae}$; S_{crit} decreases for lower contact angles and higher molecular weight

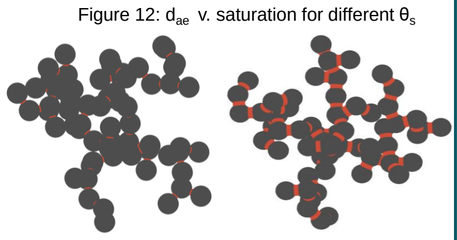

Figure 13: Krytox 16256 coating with S = 0.3, θ_s = 60° (left) And S = 0.8, θ_s = 30° (right)

Modelling perspectives

- Account for material redistribution during the original overlapping process such as sintering
- Add necking on polydisperse primary particles
- Study simultaneous coating growth and aggregate compaction as a result of capillary forces
- Advanced coating models are under development to build improved data base – highlighting the wetting performance of liquids – in order to generate realistic data and to review current model assumptions, in particular concerning particle morphology estimation, material coating, charging efficiency modelling, and global warming predictions. For example, the light interaction models used in this last field directly depend on the coating representation as the so-called ‘’lensing effect’’ is constrained by the shape of the liquid/gas interfaces

References

1. Q. Yuan et al., *Environ. Sci. Technol.* **53**, 8227-8234 (2019)
2. C. Svensson et al., *PLoS ONE* **8**, 9 (2013)
3. A. Filippov et al., *J. Colloid Interface Sci.* **229**, 1 (2000)
4. T. Thajudeen et al., *Aerosol Sci. Tech.* **46**, 11 (2012)
5. T. Johnson et al., *Aerosol Sci. Tech.* ***52***, 6 (2018)
6. J. Olfert et al., *J. Aerosol Sci.* **38**, 1 (2007)

Sponsorship and contact

This project is funded by Cambustion Ltd, Cambridge, UK

Email: amb233@cam.ac.uk (AMB), jps@cambustion.com (JPS), cj443@cam.ac.uk (CJ)